Near- and far-field Raman spectroscopic studies of nanodiamond composite films deposited by coaxial arc plasma

Ali M. Ali
Department of Applied Science for Electronics and Materials, Kyushu University

Deckert-gaudig, Tanja
Leibniz Institute of Photonic Technology (IPHT)

Egiza, Mohamed
Department of Applied Science for Electronics and Materials, Kyushu University

Deckert, Volker
Leibniz Institute of Photonic Technology (IPHT)

他

https://hdl.handle.net/2324/7183335

出版情報：Applied Physics Letters. 116 (4), pp.041601-, 2020-01-30. AIP Publishing
バージョン：

Applied Physics Letters

Near- and far-field Raman spectroscopic studies of nanodiamond composite films deposited by coaxial arc plasma

Cite as: Appl. Phys. Lett. **116**, 041601 (2020); https://doi.org/10.1063/1.5142198
Submitted: 10 December 2019 . Accepted: 06 January 2020 . Published Online: 30 January 2020

Ali M. Ali, Tanja Deckert-Gaudig, Mohamed Egiza, Volker Deckert, and Tsuyoshi Yoshitake

COLLECTIONS

F This paper was selected as Featured

ARTICLES YOU MAY BE INTERESTED IN

Enhanced-tip Raman spectroscopy used to unravel the structure of nanodiamond-carbon films
Scilight **2020**, 051109 (2020); https://doi.org/10.1063/10.0000708

Achieving high-resolution of 21nm for STED nanoscopy assisted by CdSe@ZnS quantum dots
Applied Physics Letters **116**, 041101 (2020); https://doi.org/10.1063/1.5133427

In situ wavelength tuning of quantum-dot single-photon sources integrated on a CMOS-processed silicon waveguide
Applied Physics Letters **116**, 041103 (2020); https://doi.org/10.1063/1.5129325

AIP Publishing

Applied Physics Letters ARTICLE scitation.org/journal/apl

Near- and far-field Raman spectroscopic studies of nanodiamond composite films deposited by coaxial arc plasma

Cite as: Appl. Phys. Lett. **116**, 041601 (2020); doi: 10.1063/1.5142198
Submitted: 10 December 2019 · Accepted: 6 January 2020 ·
Published Online: 30 January 2020

Ali M. Ali,[1,2,a)] Tanja Deckert-Gaudig,[3] Mohamed Egiza,[1,4] Volker Deckert,[3,5,6] and Tsuyoshi Yoshitake[1,a)]

AFFILIATIONS

[1]Department of Applied Science for Electronics and Materials, Kyushu University, Kasuga, Fukuoka 8168580, Japan
[2]Department of Physics, Al-Azhar University, Cairo 11884, Egypt
[3]Leibniz Institute of Photonic Technology (IPHT), Albert-Einsteinstr. 9, 07745 Jena, Germany
[4]Department of Mechanical Engineering, Kafrelsheikh University, Kafrelsheikh 33516, Egypt
[5]Institute of Physical Chemistry and Abbe Center of Photonics, Friedrich-Schiller-University, Jena Helmholtzweg 4, 07743 Jena, Germany
[6]Institute of Quantum Science and Engineering, Texas A&M University, College Station, Texas 77843-4242, USA

[a)]Authors to whom correspondence should be addressed: abdelgawad_ali@kyudai.jp and tsuyoshi_yoshitake@kyudai.jp

ABSTRACT

Raman spectroscopic studies on nanodiamond composite (NDC) films, comprising nano-sized diamond grains and an amorphous carbon (a-C) matrix, deposited by coaxial arc plasma deposition are challenging because the scattering of the nano-sized diamond grains competes with the strong signal of the a-C matrix. To unravel the nanocomposite structure of NDC films, both far- and near-field Raman spectroscopy were employed. Based on the comparison of visible and ultraviolet far-field Raman data, component spectra based on either nanodiamond or a-C were estimated by a peak-decomposition procedure based on band fitting. Near-field optical resolution achieved via tip-enhanced Raman spectroscopy reveals sharper peaks of both the nanodiamond and the amorphous carbon than the far-field spectra. Consequently, the peak-decomposition procedure is not required, which evidently indicates the effective detection of nanodiamond grains embedded in a-C matrices and is a direct result of the high spatial resolution that limits the number of probed grains. The size of the nanocrystals could additionally be estimated from the profile and position of a diamond peak. This work demonstrates that tip-enhanced Raman spectroscopy is a powerful nondestructive method for nanodiamond composite films, which allows direct access to parameters hitherto only available via average data.

Nanodiamond composites (NDC), i.e., diamond crystallites with diameters of less than 10 nm, are embedded in an amorphous carbon (a-C) matrix.[1,2] Owing to this composite structure, NDC films can be used in a wide range of electrical, optical, and mechanical applications.[3,4] High hardness and an extremely smooth surface of NDC films, compared with a polycrystalline diamond film, are the key to gain more and more attention for hard coating of cemented carbide and silicon substrates, which are the cores of cutting tools and electronic devices, respectively.[5] While NDC films including polycrystalline diamond films have mainly been prepared by chemical vapor deposition (CVD), recently, we have grown NDC films with grains of less than 10 nm diameter embedded in an a-C matrix by employing coaxial arc plasma deposition (CAPD).[6,7]

In our previous study, the existence of diamond crystallites in the NDC films has been examined by X-ray diffraction (XRD) using synchrotron radiation and transmission electron microscopy (TEM) in combination with a sample preparation based on focus ion beam (FIB) milling.[2,8] However, in TEM measurements, it is difficult to investigate NDC films without the graphitization of diamond nanocrystallites induced by ion bombardments during FIB processing.[9] For XRD analysis with synchrotron radiation, the measurements can be performed nondestructively, but the sample must be powdered and a distinct amount is required. Consequently, the powder has to be produced in multiple successive processes under identical conditions. A further obstacle of TEM measurements is that obtaining quantitative and microstructural information about the films is difficult.

Far-field Raman spectroscopy with multiple laser-wavelengths has already been applied to carbon-based composites.[10] Nevertheless, it is still limited to the identification of nanocarbon composites containing a diamond phase due to the following obstacles:[11] Owing to the small Raman cross section of diamond in the visible range, the Raman intensity of the characteristic diamond band is extremely weak and is often obscured by the dominating D-band of amorphous carbon.[12] Moreover, since the D- and G-bands of amorphous carbon matrices consist of several component peaks with different profiles and positions related to the various carbon configurations of the composite,[13] it is difficult to distinguish those from grain boundaries and imperfect diamond crystallites.

To overcome these limitations, tip-enhanced Raman spectroscopy (TERS) was applied in the present study. TERS is a powerful technique that enables an extremely sensitive molecular analysis down to the nanometer scale.[14,15] The high sensitivity is based on a large electric field enhancement at the apex of a metalized scanning probe tip. If such a tip is irradiated with the appropriate laser wavelength, localized surface plasmons will be generated and the Raman signal intensity of the molecules in close vicinity will be enhanced by several orders of magnitude.[14,16] In this contribution, it is demonstrated that the detection of diamond nanocrystallites embedded in an a-C matrix becomes feasible. In the first part, far-field Raman spectroscopy in the visible and the UV spectral region was employed to examine the composite structure of NDC films deposited by CAPD. In the second part, the studies were extended to the optical near-field, i.e., TERS was used for the structural investigation of nanoparticles of NDC films.

The deposition of NDC films was performed at base pressures of less than 10^{-4} Pa with a high purity graphite target (purity 99.99%, Nilaco corp. Japan). A coaxial arc plasma gun was operated at a voltage of 100 V and a repetition rate of 1 Hz. Silicon wafers (100) with a thickness of $260 \pm 10\,\mu$m (Achilles crop. Japan) were used as substrates and were placed on a substrate holder at a distance of 15 mm from the head of the coaxial arc plasma gun anodic cylinder. The films were deposited at deposition temperatures of 550, 350, and 20 °C (room temperature), and the resulting film thicknesses were estimated to be 2, 1.7, and 1.5 μm, respectively. The deposition temperature remained stable during deposition. To confirm the reproducibility of the film preparation, several samples were prepared for each condition. For reference measurements, nanodiamond powders containing crystals with a mean size of 100, 50, and 10 nm (provided from Tomei DI Japan) were used and standard Raman spectra were acquired.

For the far-field Raman excitation, wavelengths were 532 and 224 nm with maximum laser power limited to 0.5 mW and numerical aperture of 0.9 and 0.4, respectively, to avoid thermal annealing effects that induce graphitization of nanodiamond grains. The spectra were recorded with an acquisition time of 60 s and 5 accumulations. For the TERS experiments, the NDC film deposited at room temperature was placed on pre-cleaned cover slips by physical adsorption. The tip-enhanced Raman scattering setup is based on an inverted microscope (Olympus IX-70, Japan) coupled to a Raman spectrometer (Acton SP2750A, f = 750 mm, Princeton Instruments, USA). An atomic force microscope (JPK Nanowizard III, Bruker, Germany) was placed on top of the microscope to provide the precise sample and TERS-tip positioning via closed-loop controlled piezo stages. As excitation source a frequency doubled Nd-YAG laser (Spectra-Physics Excelsior, USA) at 532 nm was used at a power of 0.5 mW. The incident laser beam was focused onto the TERS tip through cover slide and the sample by an oil-immersion objective (Olympus, Japan, 60x, N. A.: 1.45). AFM cantilevers (Tap 190Al-G, Budget sensors, Germany) were thermally evaporated with 25 nm of silver and stored under argon until used as TERS probes.

Figures 1(a) and 1(b) show visible and ultraviolet (UV) Raman spectra of the bulk reference samples (standard nanodiamond powder, a-C, graphite, P = 0.5 mW, $t_{acq} = 60$ s, 5 acc). For the 50 nm and 100 nm diamond samples, the characteristic sharp signal at 1332 cm^{-1} was detected, while this band was shifted to 1325 cm^{-1} and became broader for the 10 nm diamond sample. Furthermore, the relative band intensity decreased with decreasing diamond crystal size. The observed 7 cm^{-1} downshift can be explained by a particle size-dependent local heating caused by the incident laser[17–19] and the broadening could be attributed to a phonon confinement effect and scattering in the nano-sized diamond particles.[20,21] The spectra of amorphous carbon (a-C) and graphite show two broad bands at 1350 cm^{-1} and 1580 cm^{-1} when exciting the sample with 532 nm [see Fig. 1(a)]. These signals can be assigned to the well-known D- and G-bands, respectively, and can be considered as marker bands of these carbon modifications.[22] In contrast, in the UV-Raman spectra of a-C and graphite in Fig. 1(b), only the G-band at 1587 cm^{-1} (with lower intensities compared to the visible Raman spectra) was detected. It is important to note that the D-band was not observed in

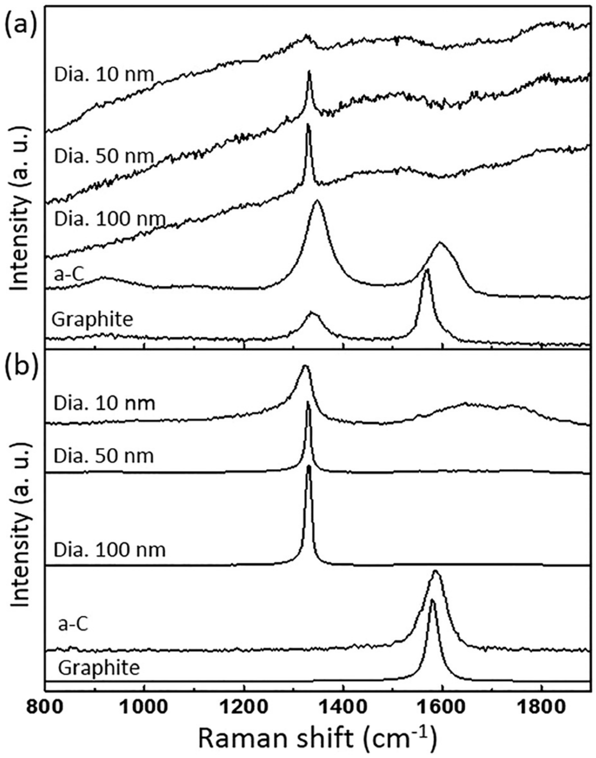

FIG. 1. Raman spectra of standard nanodiamond powder with different crystal sizes compared to amorphous carbon powder as well as graphite measured at 0.5 mW laser power and 60 s acquisition time with (a) 532 nm and (b) 224 nm excitation lasers. For better comparison, Raman spectra are plotted with an intensity offset.

the UV-Raman spectra since the Raman scattering cross section of disordered carbon bonds is known to drastically decrease in the UV range.

To investigate the structural changes of NDC films as a function of the deposition temperature, the samples were again investigated in the visible and UV region. Both conditions in Fig. 2 show similar spectral profiles (gray line) that contain broad bands between 1600 cm^{-1} and 1100 cm^{-1}, indicating contributions of the D- and G-bands, the a-C matrices, and the diamond. This observation is in agreement with previous Raman studies of carbon composite nanomaterials.[23–25] To analyze the spectra quantitatively and approach the differences between visible and UV Raman spectra, the spectra were deconvoluted into component peaks based on the obtained information in Fig. 1. In this process, the spectra were baseline-corrected between 800 and 1900 cm^{-1} and deconvoluted into peaks with Voigt functions (mixed Gaussian/Lorentzian profile) by OriginLab software.[26] The red, green, and blue lines in Fig. 2 show the band deconvolution of visible and UV excited Raman spectra of the NDC films. In the Raman spectra excited at 532 nm (shown in the inset), the bands can be assigned to diamond (red) of diamond nanocrystallites and the D- (green) and the G- (blue) band of the surrounding a-C matrices. The diamond signals are broadened and downshifted to 1325 cm^{-1}, similar to the observation obtained from the bulk nanodiamond reference sample. Furthermore, the broad D-band at 1350 cm^{-1} overlaps with the diamond band. Since the D-band is undetectable in the UV-Raman spectra, the spectra were fitted with two bands at 1325 cm^{-1} and 1600 cm^{-1} (nanodiamond and G-band). Such way, the diamond band could be separated from the G-band in the UV Raman spectra. The relative diamond band intensity increased with decreasing deposition temperature, which indicates that the growth of diamond nanocrystallites was facilitated.

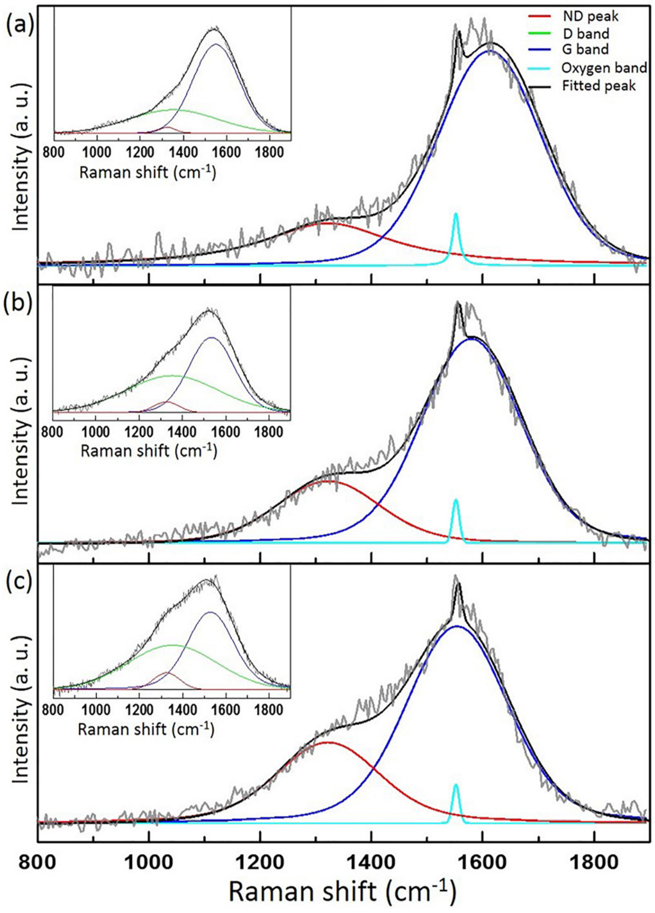

FIG. 2. Raman spectra and the respective non-linear band fits ($\lambda = 224$ nm) of NDC films deposited at temperatures of (a) 550 °C, (b) 350 °C, and (c) room temperature. Insets show the raw and fitted Raman spectra at ($\lambda = 532$ nm). Acquisition time: 60s, P = 0.5 mW. Raman spectra were baseline corrected using a linear-baseline and were fitted with three Voigt functions, respectively.

In summary, the far-field Raman experiments of NDC films in the visible range demonstrate that the diamond crystallite band cannot be clearly detected since it is usually obscured by the carbonaceous D-band. On the other hand, in the UV Raman measurements, the nanodiamond band can be extracted only by peak fitting procedures. The G-band is omnipresent, which implies that diamond crystallites are surrounded by a-C matrices.

For a detailed analysis of the NDC film nanostructure deposited at room temperature, tip-enhanced Raman spectroscopy was employed. The AFM topography of NDC nanoparticles was scanned during the TERS experiment and is shown in Figs. 3(a) and 3(b). The acquired TERS spectra correspond to the positions numbered in the AFM images of Figs. 3(a) and 3(b) and are shown in Figs. 3(c) and 3(d), respectively. The selected spectra 4–9 in Fig. 3(d) were taken from a linear point-by-point measurement on a nanoparticle in which spectra were recorded continuously every 2.5 nm ($\lambda = 532$ nm, P = 0.5 mW, $t_{acq} = 10$ s). The distance between the measurement points in Fig 3(b) was 20 nm. In the TER spectra in Fig. 3(c), the sharp diamond bands are clearly visible at 1325 cm^{-1}, which indicates that TERS can directly identify diamond in NDC nanoparticles without the need for a further deconvolution procedure. The detection of the diamond bands is in agreement with a previous work on nanodiamond particles where surface-enhanced Raman spectroscopy was used.[27,28]

The TER spectra in Fig. 3(d) demonstrate the structural change from nanodiamond to a-C when pacing along the nanoparticle. In the spectra, the Raman signal intensity of the diamond crystallites at 1325 cm^{-1} gradually decreases when the tip is moved from point 4 to point 8. Since the position of the diamond band is strongly related to the crystal size, the downshift to 1325 cm^{-1} points to the presence of a nanodiamond with a size of 10 nm or below, which is in agreement with the XRD and TEM measurements in our previous studies.[2,9] The simultaneously observed D- and G-bands around 1400 cm^{-1} and 1600 cm^{-1}, respectively, and other small bands and shoulders can be assigned to the a-carbon matrices and grain boundary of nanodiamond crystallites. Veres *et al.* and Rosenkranz *et al.* reported that the inhomogeneous intensity of D- and G-bands during sequential measurements is due to the selective enhancement of each carbon configuration,[29,30] which depends on the number of carbon layers, symmetry, and curvature of the involved carbon species.

In summary, the evident superiority of TERS for the structural evaluation of nanodiamond composite films was experimentally demonstrated by complementary far-field Raman spectroscopy at 532 and 224 nm. While the characteristic band of

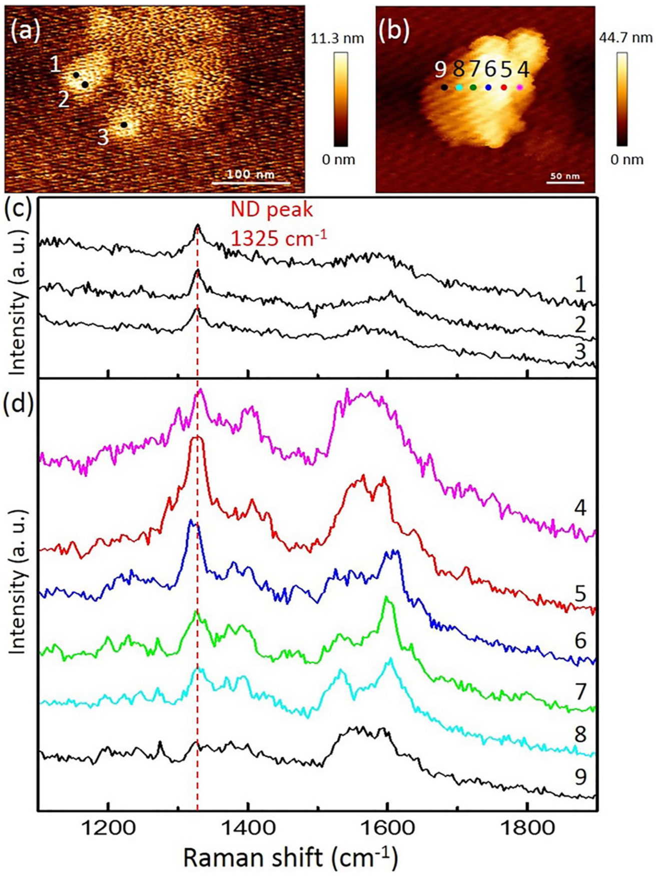

FIG. 3. (a) and (b) AFM topography images of NDC nanopartices produced from a film deposited at room temperature; (c) and (d) selected tip-enhanced Raman spectra from a line measurement on the sample as indicated in (a) and (b). $\lambda = 532$ nm, P $= 0.5$ mW, $t_{acq} = 10$ s. The presented raw TER spectra are plotted with y-offset.

diamond grains cannot clearly be detected by visible far-field Raman spectroscopy due to its overlapping with the D-band of a-C, it is possible for tip-enhanced Raman spectroscopy to clearly detect diamond peaks specific to diamond even if the grain size is smaller than 10 nm. From this, TERS would be recognized as the most powerful nondestructive method for detecting and structurally evaluating nanocarbon composited materials.

See the supplementary material for data analysis of far-field Raman spectra and more characterizations.

This research was partially financially supported by the Osawa Scientific Studies Grants Foundation, Advanced Machining Technology & Development Association, JST A-STEP Stage II (No. AS2915051S), and JSPS KAKENHI Grant No. JP19H02436. Ali M. Ali is grateful for the financial assistance provided by the Kyushu University Advanced Graduate Program in Global Strategy. V. Deckert was partly supported by the Deutsche Forschungs Gemeinschaft (DFG) via the Collaborative Research center SFB 1278 (Polytarget—Project B04).

REFERENCES

[1] H. Naragino, A. Tominaga, K. Hanada, and T. Yoshitake, “Synthesis method for ultra-nanocrystalline diamond in powder employing a coaxial arc plasma gun,” Appl. Phys. Express **8**(7), 075101 (2015).
[2] K. Hanada, T. Yoshida, Y. Nakagawa, and T. Yoshitake, “Formation of ultrananocrystalline diamond/amorphous carbon composite films in vacuum using coaxial arc plasma gun,” Jpn. J. Appl. Phys., Part 1 **49**(12R), 125503 (2010).
[3] H. Naragino, M. Egiza, A. Tominaga, K. Murasawa, H. Gonda, M. Sakurai, and T. Yoshitake, “Hard coating of ultrananocrystalline diamond/nonhydrogenated amorphous carbon composite films on cemented tungsten carbide by coaxial arc plasma deposition,” Appl. Phys. A **122**(8), 761 (2016).
[4] S. Takeichi, T. Nishiyama, M. Tabara, S. Kawawaki, M. Kohno, K. Takahashi, and T. Yoshitake, “Thermal conductivity of ultrananocrystalline diamond/hydrogenated amorphous carbon composite films prepared by coaxial arc plasma deposition,” ECS Trans. **75**(25), 27–32 (2017).
[5] S. Suarez, A. Rosenkranz, C. Gachot, and F. Mücklich, “Enhanced tribological properties of MWCNT/Ni bulk composites–Influence of processing on friction and wear behaviour,” Carbon **66**, 164–171 (2014).
[6] Y. Tang, Y. S. Li, Q. Yang, and A. Hirose, “Deposition and characterization of diamond coatings on WC-Co cutting tools with W/Al interlayer,” Diamond Relat. Mater. **19**(5–6), 496–499 (2010).
[7] P. J. Heaney, A. V. Sumant, C. D. Torres, R. W. Carpick, and F. E. Pfefferkorn, “Diamond coatings for micro end mills: Enabling the dry machining of aluminum at the micro-scale,” Diamond Relat. Mater. **17**(3), 223–233 (2008).
[8] T. Yoshitake, A. Nagano, S. Ohmagari, M. Itakura, N. Kuwano, R. Ohtani, and K. Nagayama, “Near-edge x-ray absorption fine-structure, x-ray photoemission, and Fourier transform infrared spectroscopies of ultrananocrystalline diamond/hydrogenated amorphous carbon composite films,” Jpn. J. Appl. Phys., Part 1 **48**(2R), 020222 (2009).
[9] K. Hanada, T. Nishiyama, T. Yoshitake, and K. Nagayama, “Optical emission spectroscopy of deposition process of ultrananocrystalline diamond/hydrogenated amorphous carbon composite films by using a coaxial arc plasma gun,” Diamond Relat. Mater. **19**(7–9), 899–903 (2010).
[10] C. Casiraghi, A. C. Ferrari, and J. Robertson, “Raman spectroscopy of hydrogenated amorphous carbons,” Phys. Rev. B **72**(8), 085401 (2005).
[11] V. Mochalin, S. Osswald, and Y. Gogotsi, “Contribution of functional groups to the Raman spectrum of nanodiamond powders,” Chem. Mater. **21**(2), 273–279 (2009).
[12] S. Prawer, K. W. Nugent, D. N. Jamieson, J. O. Orwa, L. A. Bursill, and J. L. Peng, “The Raman spectrum of nanocrystalline diamond,” Chem. Phys. Lett. **332**(1–2), 93–97 (2000).
[13] M. Veres, M. Füle, S. Toth, M. Koos, and I. Pocsik, “Surface enhanced Raman scattering (SERS) investigation of amorphous carbon,” Diamond Relat. Mater. **13**(4–8), 1412–1415 (2004).
[14] T. Deckert-Gaudig, A. Taguchi, S. Kawata, and V. Deckert, “Tip-enhanced Raman spectroscopy—from early developments to recent advances,” Chem. Soc. Rev. **46**(13), 4077–4110 (2017).
[15] P. Verma, “Tip-enhanced Raman spectroscopy: Technique and recent advances,” Chem. Rev. **117**(9), 6447–6466 (2017).
[16] A. B. Zrimsek, N. Chiang, M. Mattei, S. Zaleski, M. O. McAnally, C. T. Chapman, and R. P. Van Duyne, “Single-molecule chemistry with surface-and tip-enhanced Raman spectroscopy,” Chem. Rev. **117**(11), 7583–7613 (2017).
[17] C. F. Ruiz-Valdez, V. Chernov, R. Meléndrez, S. Álvarez-García, K. Santacruz-Gómez, D. Berman-Mendoza, and M. Barboza-Flores, “Raman and thermoluminescence studies of HPHT Synthetic nanodiamond powders,” Phys. Status Solidi A **215**(22), 1800267 (2018).
[18] P. W. May, J. A. Smith, and K. N. Rosser, “785 nm Raman spectroscopy of CVD diamond films,” Diamond Relat. Mater. **17**(2), 199–203 (2008).
[19] X. Z. Zhao, K. A. Cherian, R. Roy, and W. B. White, “Downshift of Raman peak in diamond powders,” J. Mater. Res. **13**(7), 1974–1976 (1998).
[20] V. N. Mochalin, O. Shenderova, D. Ho, and Y. Gogotsi, “The properties and applications of nanodiamonds,” Nat. Nanotechnol. **7**(1), 11 (2012).
[21] M. Popov, V. Churkin, A. Kirichenko, V. Denisov, D. Ovsyannikov, B. Kulnitskiy, and V. Blank, “Raman spectra and bulk modulus of

nanodiamond in a size interval of 2–5 nm," Nanoscale Res. Lett. **12**(1), 561 (2017).

[22] T. Sharda, T. Soga, T. Jimbo, and M. Umeno, "Growth of nanocrystalline diamond films by biased enhanced microwave plasma chemical vapor deposition," Diamond Relat. Mater. **10**(9–10), 1592–1596 (2001).

[23] T. Hara, T. Yoshitake, T. Fukugawa, H. Kubo, M. Itakura, N. Kuwano, and K. Nagayama, "Ultrananocrystalline diamond prepared by pulsed laser deposition," Diamond Relat. Mater. **15**(4–8), 649–653 (2006).

[24] X. Xiao, J. Birrell, J. E. Gerbi, O. Auciello, and J. A. Carlisle, "Low temperature growth of ultrananocrystalline diamond," J. Appl. Phys. **96**(4), 2232–2239 (2004).

[25] A. Nagano, T. Yoshitake, T. Hara, and K. Nagayama, "Optical properties of ultrananocrystalline diamond/amorphous carbon composite films prepared by pulsed laser deposition," Diamond Relat. Mater. **17**(7–10), 1199–1202 (2008).

[26] J. Cebik, J. K. McDonough, F. Peerally, R. Medrano, I. Neitzel, Y. Gogotsi, and S. Osswald, "Raman spectroscopy study of the nanodiamond-to-carbon onion transformation," Nanotechnology **24**(20), 205703 (2013).

[27] E. Perevedentseva, A. Karmenyan, P. H. Chung, and C. L. Cheng, "Surface-enhanced Raman spectroscopy of nanodiamond particles on silver," J. Vacuum Sci. Technol., B **23**(5), 1980–1983 (2005).

[28] S. Osswald, G. Yushin, V. Mochalin, S. O. Kucheyev, and Y. Gogotsi, "Control of sp2/sp3 carbon ratio and surface chemistry of nanodiamond powders by selective oxidation in air," J. Am. Chem. Soc. **128**(35), 11635–11642 (2006).

[29] M. Veres, S. Tóth, and M. Koós, "Grain boundary fine structure of ultrananocrystalline diamond thin films measured by Raman scattering," Appl. Phys. Lett. **91**(3), 031913 (2007).

[30] A. Rosenkranz, L. Freeman, B. Suen, Y. Fainman, and F. E. Talke, "Tip-enhanced Raman spectroscopy studies on amorphous carbon films and carbon overcoats in commercial hard disk drives," Tribol. Lett. **66**(2), 54 (2018).